The velocity synchronous discrete Fourier transform for order tracking in the field of rotating machinery

P. Borghesani *, P. Pennacchi, S. Chatterton, R. Ricci

Politecnico di Milano, Dipartimento di Meccanica, via la Masa 1, 20156 Milano, Italy

Received 18 June 2012
Received in revised form
8 March 2013
Accepted 31 March 2013

1. Introduction

Most signals measured in the field of machine condition monitoring present strong, often dominant, harmonic components, synchronous with the shaft rotation. For instance, the analysis of signal for the diagnostics of rotors [1] and gears [2] is usually based on integer multiples of the shaft velocity. Considering that also the cyclostationary components, the second biggest class in machine diagnostics, present cyclic frequencies strictly related to the shaft velocity [3], it is clear that the monitoring of rotating machineries is by far more effective if analyses are performed in the *angular domain* of the shaft rotation, rather than in *time domain*. The same conclusion is valid for the order domain, the spectral counterpart of the angular domain (measured in *n per revolution*, *n*X), which is always preferred to the "Hertzian" frequency domain.

The idea of synchronously sampling mechanical signals came from the field of electronics and telecommunications, where, a wide and detailed literature was available starting from the '60s, see for instance [4,5] and [6]. Prior to the diffusion of cheap micro-processors the most feasible option consisted in electronic circuits able to generate triggering waves for the

* Corresponding author. Tel.: +39 022 399 8486.
E-mail address: pietro.borghesani@mail.polimi.it (P. Borghesani).

acquisition system, phase-locked with a speed sensor installed on the machine [7]. Thanks to these hardware systems, the sampling of the signal could be performed directly in the angular domain, i.e. at constant shaft angular increments, instead of constant time intervals.

The availability of cheap digital signal processors has made a second option more economically appealing to obtain signals in the angular domain. It consists in digitally processing the signal in order to obtain the domain transformation. In this way, the complexity of the hardware is significantly reduced, and the system becomes much more flexible for modifications. The first attempts in this direction started in the late 80s [8], to reach the most significant results in the 90s, with the works of Fyfe and Munck [9], Stander and Heyns [10], Vold and Leuridan [11], Blough, Brown and Vold [12]. The different approaches may be grouped in three big families of order tracking techniques: the *resampling methods*, the *Kalman filter based methods* and the *transform based methods*.

The resampling methods, or *computed order tracking* (COT), are the most intuitive approach: they work mainly in time domain, interpolating the signal to obtain a result which should represent a signal sampled by a hardware-synchronized acquisition system. The second family is based on non-casual filtering operations [16], which, in some implementations, can be recursively adjusted [17]. The third family of order tracking techniques is based on integral transforms, able to extract, with some degree of accuracy, the order domain information directly from the time-domain signal. Such transforms are generally derived from the Fourier transform, with proper modifications of the kernel [12]. This paper focuses on this last family of order tracking techniques, which present the advantage of a direct passage from the signal sampled uniformly in time domain to the order spectrum. In particular the paper introduces a new transform, the *velocity synchronous discrete Fourier transform* (VSDFT), exploiting the estimate of the instantaneous angular speed (IAS) to perform the order tracking. The estimation of the instantaneous angular speed [13–15] is not the focus of this paper, which deals with its use for the aforementioned purpose of order tracking.

2. Order tracking: a multi-domain problem

The *order spectrum*, the angular counterpart of the common frequency spectrum, is obtained by Fourier transforming the signal from the angular domain:

$$X(\Omega) = \int_{-\infty}^{+\infty} x(\theta) e^{-j\Omega\theta} d\theta \tag{1}$$

To practically implement this operation directly by means of *discrete Fourier transform* (DFT), a (synchronous) constant angular sampling should be implemented. However acquisition systems are seldom programmed to acquire data in a synchronous way and signal are usually sampled at constant time intervals, irrespective of the actual instantaneous velocity of the shaft.

Among the different techniques developed in literature to overcome this problem, two are worth mentioning to introduce the technique proposed in this paper. The aforementioned COT focuses on the modification of the signal $x(t)$ itself, transforming it to the angular domain by means of numerical interpolations. The resulting signal $x(\theta)$ is sampled at constant angular increments and can directly undergo the digitalized form of the transformation of Eq. (1), consisting in practice of a common DFT in the new angular domain:

$$X[k] = \frac{1}{N} \sum_{n=0}^{N-1} x[n\Delta\theta] e^{-j\Omega[k]n\Delta\theta} \tag{2}$$

where $\Delta\theta$ and N are respectively the angular resolution and the number of samples of the interpolated signal $x(\theta)$, and $\Omega[k]$ the vector of orders for the representation of the order spectrum. The second technique, belonging to the family of integral transforms for order tracking and proposed by Blough et al. [12], exploits the possibility of changing the kernel of the transformation itself, to pass directly from the time domain to the order domain $\{\Omega\}$. Such DSP technique, a particular case of the chirp-z transform, is called *time variant Fourier transform* (TVDFT), whose expression is the following:

$$\mathrm{TVDFT}[k] = \frac{1}{N} \sum_{n=1}^{N} x[n\Delta t] e^{-j\Omega[k] \int_0^{n\Delta t} \omega[n] dt} \tag{3}$$

The modified kernel, characterized by the instantaneous frequency of the tachometer ω, allows processing the signal $x[n\Delta t]$ without prior resampling. However, such transform shows limits for highly variable shaft speeds and is characterized by a set of non-orthogonal kernels. Blough proposed the introduction of an *orthogonality compensation matrix* (OCM) to partially correct this problem [18].

Significant improvements can be obtained reconsidering the theoretical basis of the domain transformation, restarting from Eq. (1), at the basis of COT, and operating a change of variable in the domain of integration:

$$X(\Omega) = \int_{-\infty}^{+\infty} x(\theta(t)) e^{-j\Omega\theta} \frac{d\theta}{dt} dt \tag{4}$$

The derivative of the angular rotation of the shaft is measured by the tachometer signal ω, thus the expression is simplified in the following:

$$X(\Omega) = \int_{-\infty}^{+\infty} x(t)\omega(t)e^{-j\Omega\theta(t)}dt \tag{5}$$

This way of interpreting the transformation has the advantage of sharing the same strong analytical basis of COT, without the need of passing through the interpolation step. Moreover, orthogonality of the kernels is verified, thanks to the implicit passage to the angular domain, operated by ω, i.e. the kernels are orthogonal with respect to ω:

$$\begin{aligned} E(\Omega) &= \int_{-\infty}^{+\infty} e^{-j\Omega_k\theta(t)}\omega(t)e^{j\Omega_l\theta(t)}dt \\ &= \int_{-\infty}^{+\infty} e^{-j\Omega_k\theta}e^{j\Omega_l\theta}\frac{d\theta}{dt}dt = \delta_{kl} \end{aligned} \tag{6}$$

where δ_{kl} represent Kronecker's delta function.

In practice, this expression is realized by the following DSP transform, named *velocity synchronous Fourier transform* (VSDFT):

$$\mathrm{VSDFT}[k] = \frac{\Delta t}{\Theta}\sum_{n=0}^{N-1} x[n\Delta t]\omega[n\Delta t]e^{-j\Omega[k\Delta\Omega]\theta[n\Delta t]} \tag{7}$$

where both time and order domain have been discretized. The normalization variable Θ corresponds to the acquisition time window T in the angular domain and its role will be discussed in detail later, along with the effects of discretization.

3. Time domain discretization: a comparison with the traditional TVDFT

To assess the improvement of this newly proposed transform, with respect to the traditional TVDFT, it is necessary to analyze the effect of the sampling on the evaluation of the order spectrum. In order to do that, it is better to rewrite Eq. (7), restoring a continuous dependence on Ω:

$$\mathrm{VSDFT}_x(\Omega) = \frac{\Delta t}{\Theta}\sum_{n=0}^{N-1} x[n\Delta t]\omega[n\Delta t]e^{-j\Omega\theta[n\Delta t]} \tag{8}$$

The discretized Eq. (8) can be represented multiplying the continuous time expression of Eq. (5) by a finite Dirac comb with period Δt:

$$\mathrm{VSDFT}_x(\Omega) = \frac{\Delta t}{\Theta}\sum_{n=0}^{N-1}\int_{-\infty}^{+\infty} x(t)\omega(t)e^{-j\Omega\theta(t)}\delta(t-n\Delta t)dt \tag{9}$$

By passing to the angular domain, thanks to the term $\omega(t)$, and exploiting the convolution theorem (in the angular-order domains), the following expression is obtained:

$$\mathrm{VSDFT}_x(\Omega) = X(\Omega)\otimes\frac{\Delta t}{\Theta}\sum_{n=0}^{N-1}\int_{-\infty}^{+\infty}\delta(t-n\Delta t)e^{-j\Omega\theta(t)}d\theta \tag{10}$$

where $X(\Omega)$ represents the Fourier transform of the continuous time signal, as obtained analytically by Eq. (5). The integral can be solved in the time domain by making $\omega(t)$ explicit again and exploiting the properties of Dirac's delta integrated over the whole time domain:

$$\mathrm{VSDFT}_x(\Omega) = X(\Omega)\otimes\frac{\Delta t}{\Theta}\sum_{n=0}^{N-1}\omega[n\Delta t]e^{-j\Omega\theta[n\Delta t]} \tag{11}$$

It can be noticed that the last term of the convolution is nothing but a VSDFT of the constant unitary value, therefore:

$$\mathrm{VSDFT}_x(\Omega) = X(\Omega)\otimes\mathrm{VSDFT}_1(\Omega) \tag{12}$$

By means of similar steps it is possible to demonstrate that the discretization in the traditional TVDFT results in the following:

$$\begin{aligned} \mathrm{TVDFT}_x(\Omega) &= X(\Omega)\otimes\frac{1}{N}\sum_{n=0}^{N-1} e^{-j\Omega\theta[n\Delta t]} \\ &= X(\Omega)\otimes\mathrm{TVDFT}_1(\Omega) \end{aligned} \tag{13}$$

The sums of Eqs. (11) and (13), convolved to the order spectrum $X(\Omega)$ of the actual signal, are the key drivers of the quality of the results of the two transforms; therefore they deserve a deeper analysis. In particular it is desirable that the result of those summations is as close as possible to an impulsive function with unitary value in $\Omega=0$ and null value all over the remaining order domain, in order to avoid short and long range leakage [19].

By the assumption of calculating instantaneous speed as a finite difference of the angular position, and replacing for the sake of simplicity the form $[n\Delta t]$ with the subscript n, $\mathrm{VSDFT}_1(\Omega)$ can be written as:

$$\mathrm{VSDFT}_1(\Omega) = \frac{1}{\Theta}\sum_{n=0}^{N-1} e^{-j\Omega\theta_n}\cdot\Delta\theta_n \tag{14}$$

where the angular increment $\Delta\theta_n$ is calculated by:

$$\Delta\theta_n = \theta_{n+1} - \theta_n \tag{15}$$

and the normalization factor, representing the angular period will be

$$\Theta = \sum_{n=0}^{N-1} \Delta\theta_n \tag{16}$$

Eq. (14) appears as a numerical integration of the imaginary exponential function in the angular domain, in the form of a Riemann sum with non-uniform intervals $\Delta\theta_n$. In a similar way, it is possible to consider the traditional transform of the unitary constant $\mathrm{TVDFT}_1(\Omega)$ as a numerical integration in the time domain of the same imaginary exponential function:

$$\mathrm{TVDFT}_1(\Omega) = \frac{1}{T}\sum_{n=0}^{N-1} e^{-j\Omega\theta_n}\cdot\Delta t \tag{17}$$

Despite the apparent advantage of interval uniformity in the Riemann sum of Eq. (17), the comparison of the two numerical integrations favors the $\mathrm{VSDFT}_1(\Omega)$: the periodicity of the exponential in the order domain guarantees that the sum converges to zero with a decrease of the maximum interval dimension, given that the orders Ω are chosen to have an integer number of periods of the exponential functions (this issue will be discussed in detail in the next section). On the contrary, no guarantee of null result is given for the integration performed in time domain (TVDFT), where the exponential function shows a non-periodic behavior.

This conclusion is even more evident if drawn from the numerical example of Fig. 1, where a chirp sinusoidal signal, representing the exponential function, is integrated in the two domains after a constant time interval sampling. It is clear that the Riemann sum represented by the yellow histograms of Fig. 1(a) will give a non-null result, even for very fine time resolution of the sampling, whereas the Riemann sum of Fig. 1(b) tends to zero with a refinement of the time resolution.

The example of Fig. 1(b) highlights the precise nature of the integration performed by VSDFT, with the angular increment calculated as by Eq. (15): a non-uniform Riemann sum with a top-left corner approximation [20]. Thus the error in the evaluation of a continuous integral with Eq. (17) will be:

$$\left|\frac{1}{\Theta}\int_0^{\Theta} e^{-j\Omega\theta}\cdot d\theta - \mathrm{VSDFT}_1(\Omega)\right| \le \frac{\Omega}{2}\max_{[0,N-1]}(\theta_{n+1}-\theta_n) \tag{18}$$

If a proper order domain discretization is chosen, so that for each Ω_k the imaginary exponential function shows an integer number of orders, the integral on the left hand side of Eq. (18) will be null, and the absolute value of the Riemann sum result will be upper bounded by the error itself:

$$|\mathrm{VSDFT}_1(\Omega)| \le \frac{\Omega}{2}\max_{[0,N-1]}\Delta\theta_n \tag{19}$$

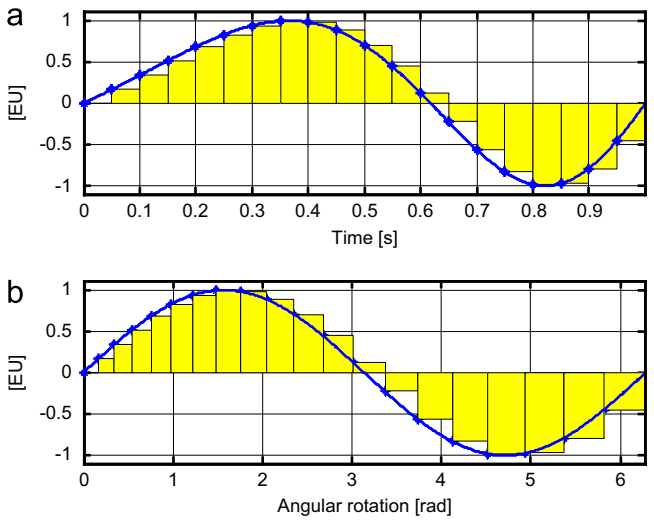

Fig. 1. Numerical integration of a chirp signal: (a) in time domain—TVDFT, (b) in angular domain—VSDFT.

A similar result is obtained by considering the $\mathrm{VSDFT}_1(\Omega)$ as a uniform Riemann sum in the time-domain, weighted by instantaneous velocity:

$$\mathrm{VSDFT}_1(\Omega) = \frac{1}{\Theta}\sum_{n=0}^{N-1}\{\omega[n]e^{-j\Omega\theta[n]}\}\cdot\Delta t \tag{20}$$

In this case the upper bound is expressed by:

$$\left|\mathrm{VSDFT}_1(\Omega)\right| \le \frac{T\Delta t}{2\Theta}\max_{[0,T]}\frac{d}{dt}\left\{\omega(t)e^{-j\Omega\theta(t)}\right\} \tag{21}$$

which, neglecting angular acceleration and discretizing, is approximated by:

$$\left|\mathrm{VSDFT}_1(\Omega)\right| \le \frac{T\Omega\Delta t}{2\Theta}\max_{[0,N-1]}\omega_n^2 \tag{22}$$

It can be seen that error bounds found in Eqs. (19) and (22) are by far conservative for the lower orders Ω, for which the angular period of the exponential function is sufficiently longer than the maximum integration interval $\Delta\theta$. In this case, it is possible to say that the periodic behavior of the function will make the single interval errors to mutually eliminate; thus the error of the whole numerical integration performed by $\mathrm{VSDFT}_1(\Omega)$ will be less than the maximum error within one interval of the numerical integration:

$$\left|\mathrm{VSDFT}_1(\Omega)\right| \le \frac{\Omega}{2\Theta}\max_{[0,N-1]}\Delta\theta_n^2 \tag{23}$$

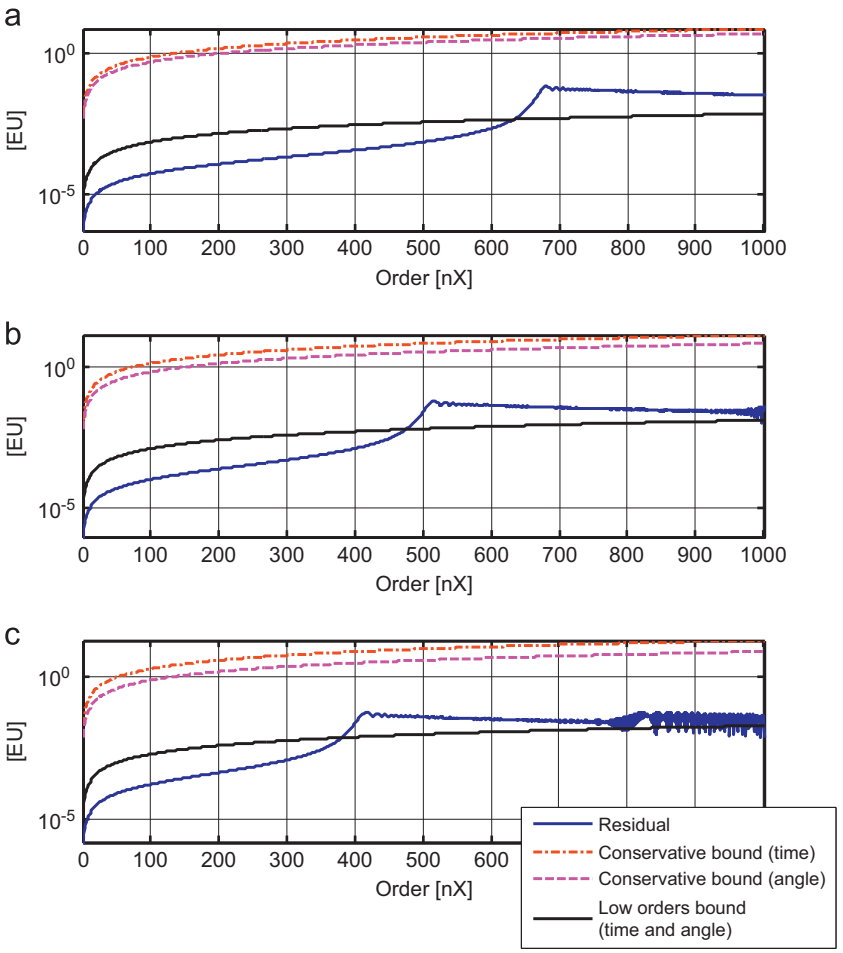

Fig. 2. Residuals of $\mathrm{VSDFT}_1(\Omega)$ (VSDFT of the constant unitary value) and corresponding analytical upper bounds: (a) constant angular acceleration, (b) linearly increasing acceleration, (c) quadratically increasing acceleration. Bounds are representing Eq. (22) for the conservative bound in time domain, Eq. (19) for the conservative bound in angular domain and Eqs. (23) and (24) for the low orders bound.

by similar considerations, a similar expression can be obtained in time domain:

$$\left|\mathrm{VSDFT}_1(\Omega)\right| \leq \frac{\Omega \Delta t^2}{2\Theta} \max_{[0,N-1]} \omega_n^2 \tag{24}$$

In Fig. 2, examples with numerical evaluations of $\mathrm{VSDFT}_1(\Omega)$ are provided for a shaft undergoing: uniform acceleration (a), linearly increasing acceleration (b) and quadratically increasing acceleration (c). These three examples, meant to be a verification of the theoretical conclusions for increasingly harsher speed profiles, show that the conservative limits, calculated in (19) and (22), are equally valid in all the cases. On the other hand, the range of orders in which the residual is limited by the more restrictive upper bound of Eqs. (23) and (24) is shrinking as the variability of speed profile increases, due to higher degrees in the acceleration law. A quantitative limit for the order range in which Eqs. (23) and (24) are valid is discussed in the next section, and is strictly related to the maximum angular increment $\Delta\theta_n$. Moreover it will be shown that

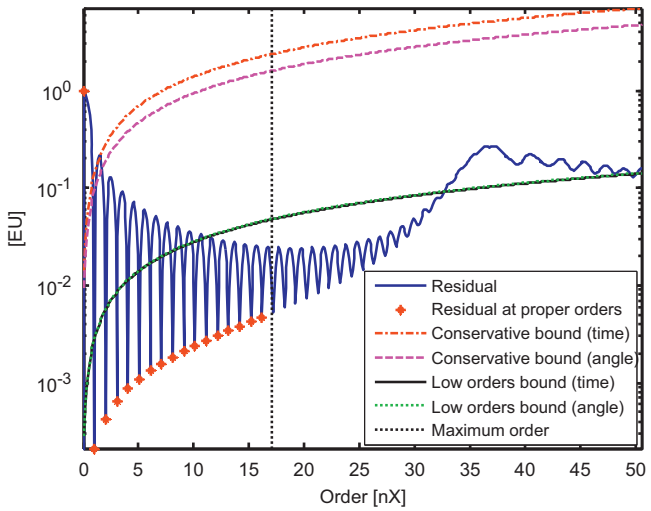

Fig. 3. Residuals of $\mathrm{VSDFT}_1(\Omega)$ (VSDFT of the constant unitary value) and corresponding analytical upper bounds: bounds are representing Eq. (22) for the conservative bound in time domain, Eq. (19) for the conservative bound in angular domain and Eqs. (23) and (24) for the low orders bound.

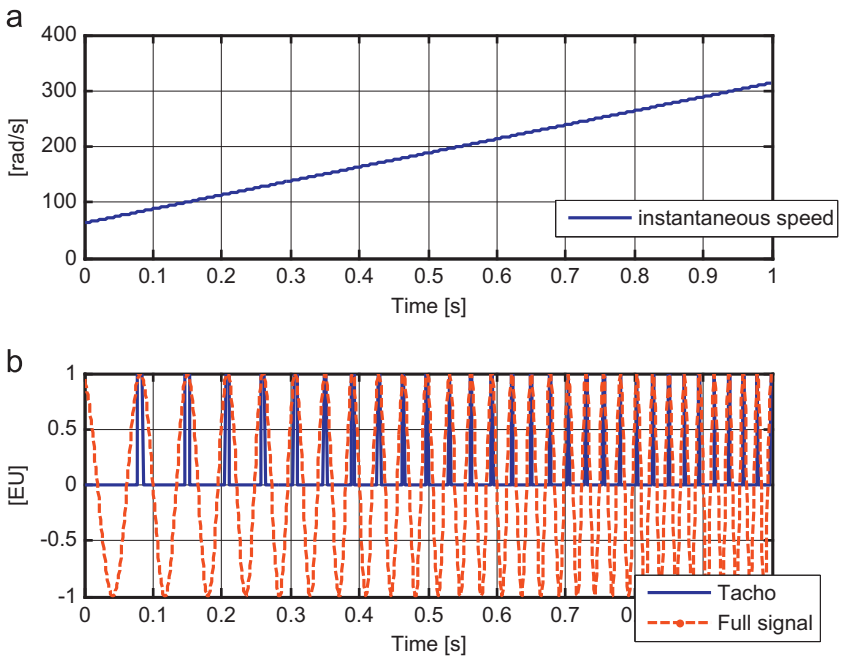

Fig. 4. Numerical simulation: (a) shaft speed profile, (b) simulated 1X tachometer (blue line), simulated sampled signal (red dots) and windowed signal (greed dotted line). (For interpretation of the references to color in this figure legend, the reader is referred to the web version of this article.)

the limit is applicable all over the significant order range, as delimited by the sampling theorem. From the diagrams of Fig. 2 it is possible to conclude also that the upper bounds obtained from time domain and angular domain quantities are equivalent, especially for the lower orders limit.

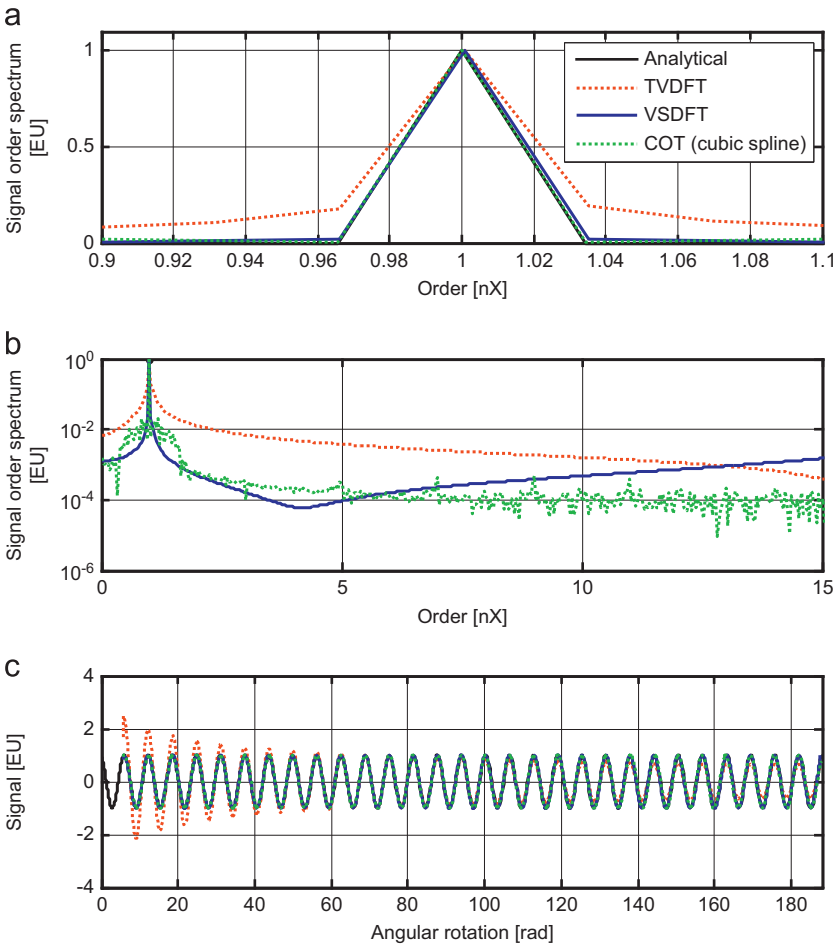

Fig. 5. Numerical simulation results: (a) order spectrum zoom with linearly scaled *y*-axis, (b) log-scale order spectrum, (c) angular domain signals reconstructed by means of inverse DFT.

Fig. 6. Experimental test rig 1.

4. Order domain discretization: choosing a proper vector

The correct discretization of the order domain for the VSDFT transform, anticipated in the previous paragraph, consists in choosing the optimal order resolution $\Delta\Omega$ and the bounds for the Ω vector. The optimal resolution can be derived by some easy analytical steps starting from Eq. (5) and introducing the rectangular observation window rect(t):

$$\mathrm{rect}(t)=\begin{cases}1 & -1/2<t<1/2\\ 1/2 & t=\pm 1/2\\ 0 & \text{otherwise}\end{cases} \tag{25}$$

The continuous time signal, observed in the time interval $0\le t\le T$ is:

$$x_W(t)=x(t)\cdot\mathrm{rect}\left(\frac{t}{T}-\frac{1}{2}\right) \tag{26}$$

Thus, Eq. (5) results in:

$$X_W(\Omega)=\int_{-\infty}^{+\infty}x(t)\mathrm{rect}\left(\frac{t}{T}-\frac{1}{2}\right)e^{-j\Omega\theta}\omega(t)dt \tag{27}$$

Operating a variable change from the time domain to the angular domain, the form of the rectangular window does not change, resulting in the following:

$$X_W(\Omega)=\int_{-\infty}^{+\infty}x(\theta)\mathrm{rect}\left(\frac{\theta}{\Theta}-\frac{1}{2}\right)e^{-j\Omega\theta}d\theta \tag{28}$$

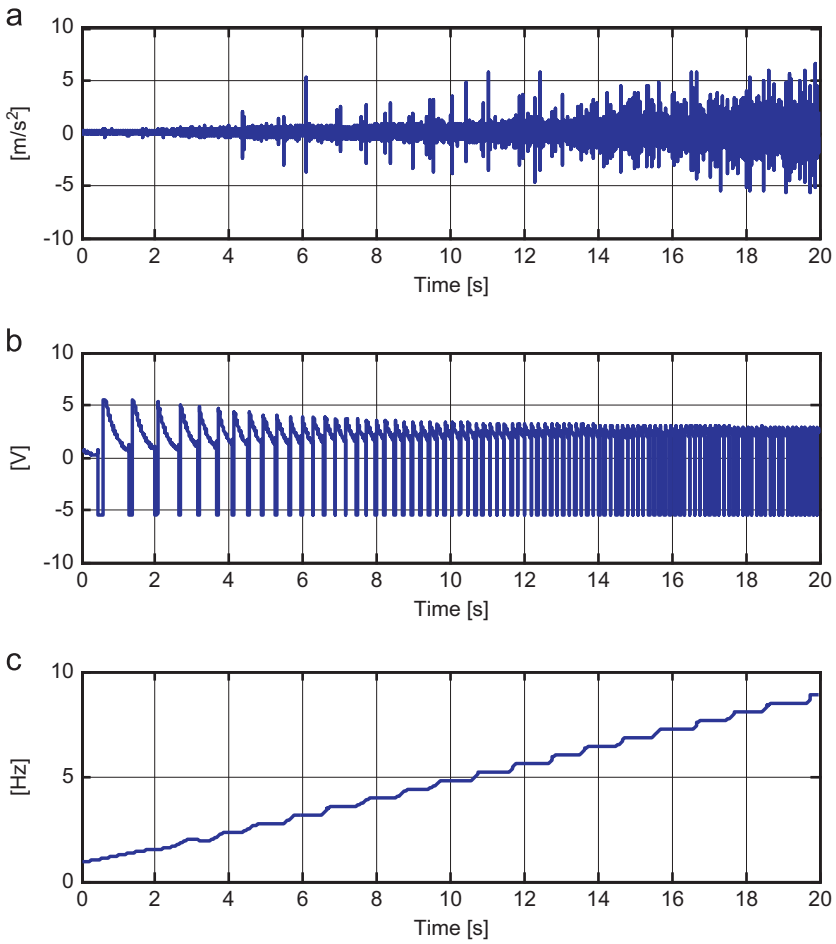

Fig. 7. Experimental test rig 1: (a) raw accelerometer signal, (b) raw tachometer signal, (c) velocity profile obtained from tachometer signal.

Thus, the angular domain Fourier transform $X_W(\Omega)$ is obtained by the convolution of $X(\Omega)$ with the transform of the rectangular window:

$$\begin{aligned} \mathrm{RECT}(\Omega) &= \int_{-\infty}^{+\infty} \mathrm{rect}\left(\frac{\theta}{\Theta}-\frac{1}{2}\right) e^{-j\Omega\theta} d\theta \\ &= \frac{1}{j\sqrt{2\pi}} \frac{e^{j\Theta\Omega}}{\Omega} \end{aligned} \tag{29}$$

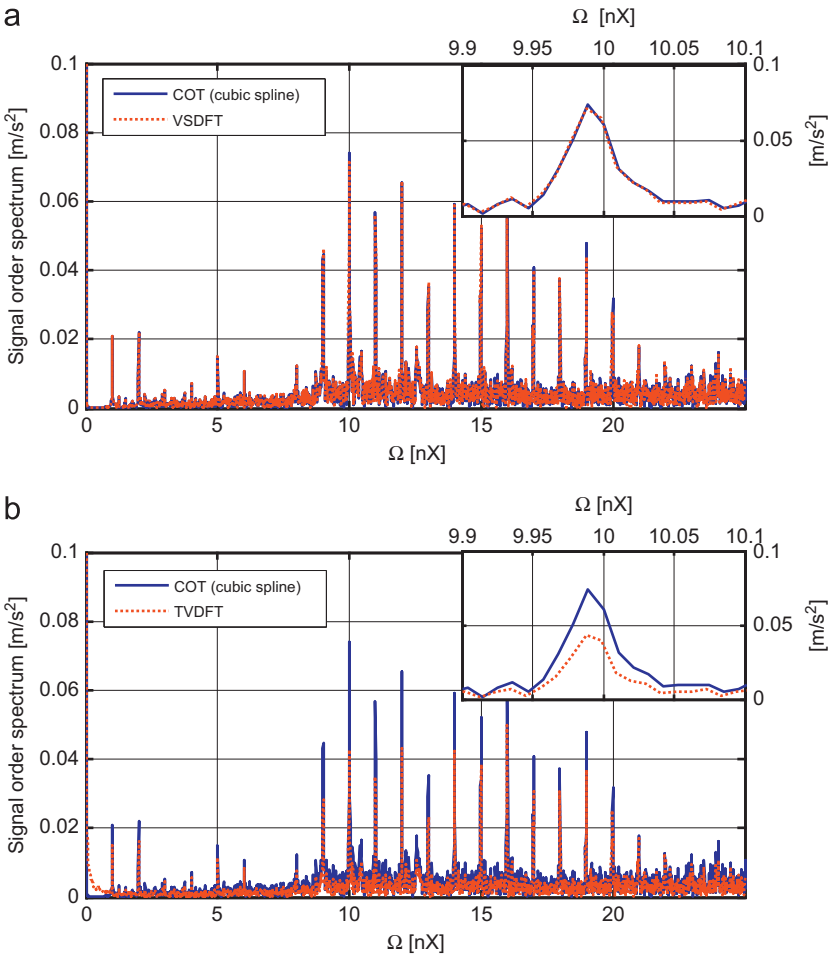

Fig. 8. Experimental test rig 1: result of the application of VSDFT (a) and TVDFT (b) to experimental data and comparison with cubic spline COT.

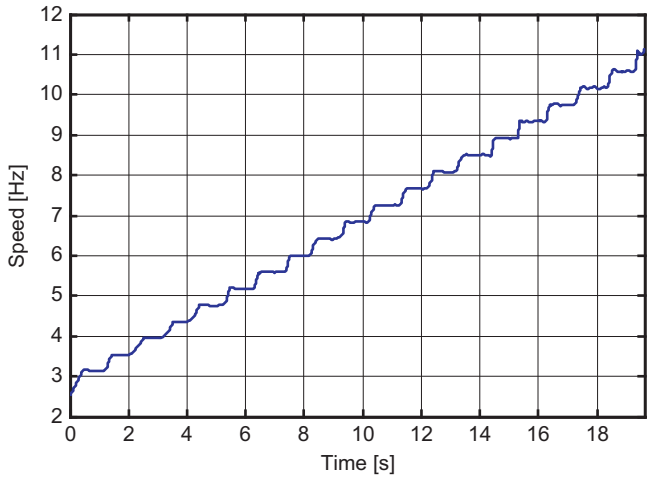

Fig. 9. Experimental test rig 1: speed transient for the calculation of the order spectrogram.

This function presents a series of lobes, characteristic of the corresponding frequency domain Fourier transformed rectangular function [19], with roots in:

$$\Omega = \frac{2n\pi}{\Theta} \quad n \neq 0 \tag{30}$$

Therefore Eq. (28) has the following expression:

$$X_W(\Omega) = \frac{1}{j\sqrt{2\pi}} \frac{e^{j\Theta\Omega}}{\Omega} \otimes X(\Omega) \tag{31}$$

In order to reduce leakage errors it is therefore suitable to choose an order domain resolution $\Delta\Omega$ of:

$$\Delta\Omega = \frac{2\pi}{\Theta} \tag{32}$$

This choice will result in a series of imaginary exponential functions with an integer number of periods in the angular window Θ, as prescribed already in the previous section.

Limits for the order vectors, at which the VSDFT should be calculated, are similar to the ones of Fourier transform, as derived from the sampling theorem:

$$\Omega_{\max} = \frac{\pi}{\sup\limits_{0 \le n < N} \Delta\theta_n} \tag{33}$$

In Fig. 3 the effect of the choice of the order domain is shown on $\mathrm{VSDFT}_1(\Omega)$ (blue line). It is clear that leakage is minimized for the order interval choice of Eq. (32) (red marks) and that the shape of the resulting function follows the theoretical upper bound laws, Eqs. (23) and (24), only up to the sampling theorem limit indicated by Eq. (33) (black dotted line).

5. Numerical simulations

A numerical simulation of a chirp signal has been performed to have a first practical validation of the new technique, both in absolute terms and in comparison with the results of COT and TVDFT. The simulated signal (red dotted line in Fig. 4 (b)) has been synchronized with the first harmonics of the shaft (order 1), whose rotational speed has been set to increase linearly (constant acceleration) from 10 to 50 Hz in 1 s as shown in Fig. 4(a). A sampling frequency of 1 kHz has been set for the time discretization, and a simulated tachometer signal (blue line in Fig. 4(b)), providing a 1X impulse has been used to perform COT. The signal has been windowed with rectangular window using the first and the last impulses of the tachometer, to obtain an integer number of revolutions, excluding the very first and last samples.

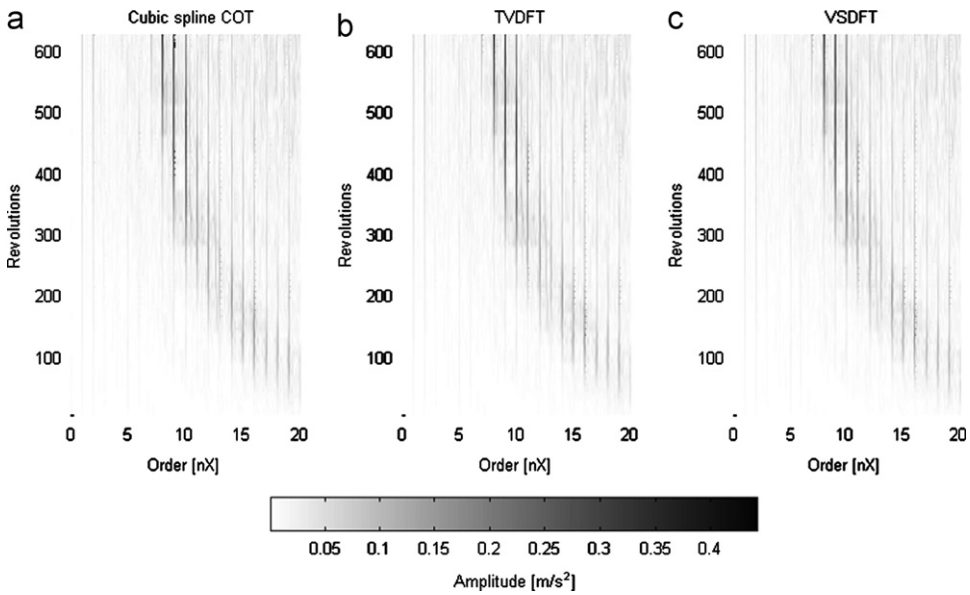

Fig. 10. Experimental test rig 1, order spectrum calculated by means of: (a) cubic spline COT, (b) TVDFT, (c) VSDFT. Sliding observation window length set to 10 revolutions; overlap of 8 revolutions.

The results of the application of COT, TVDFT and VSDFT are shown in Fig. 5, displaying the transformed signal in order domain (a–b) and the reconstructed signal in the angular domain (c), obtained by inverse transforming from the order domain through a common inverse DFT.

The quality of VSDFT is comparable to the one of COT both in the order domain and in time domain, where no significant deviation from the signal calculated analytically is noticeable. On the contrary, TVDFT results in a high leakage in the order spectrum and a numerical distortion in the amplitude of the signal, once transformed back to the angular domain. This is due to the absence of the corrective term of instantaneous speed in the transform.

6. Experimental application

The test rig used for the first experimental example is shown in Fig. 6. It has been designed for testing gears and bearings of small dimension. It consists of a brushless electric motor, controlled by means of an inverter, coupled to a spiral bevel gearbox with orthogonal axis. The gear consists of a 17 teeth pinion coupled with a 34 teeth gear, resulting in a gear ratio of 2. The output shaft of the gearbox is connected by a flexible joint to the main shaft, where the bearing under test is installed. Two additional healthy roller bearings, acting as supports, and a loading device, consisting of a preloaded spring and a regulating screw, are mounted on the main shaft. At the other end of the main shaft, another flexible joint transmits torque to a second brushless motor, similar to the first, but functioning as a brake.

The following sensors are installed on the test rig: a 1x revolution tachometric signal on the main shaft and two identical PCB IEPE piezoelectric accelerometers, mounted on the housing of the bearing under test in two mutually orthogonal radial directions.

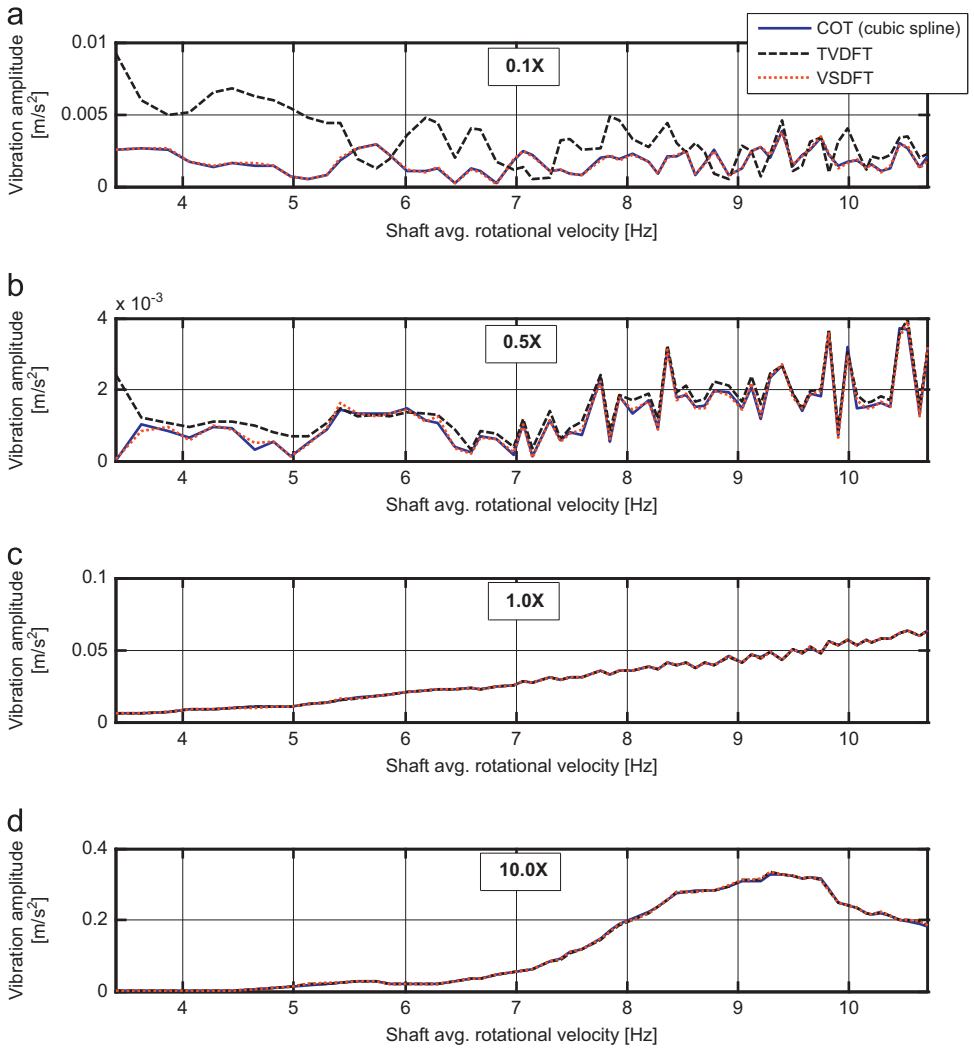

Fig. 11. Experimental test rig 1, amplitude of selected harmonics as a function of shaft speed: (a) 0.1 × , (b) 0.5 × , (c) 1 × , (d) 10 × .

The shaft rotating velocity during the test has been increased manually, resulting in the profile shown in Fig. 7(c), obtained by interpolation of the raw tachometer signal of Fig. 7(b). The profile is characterized by small fluctuations around an almost uniform acceleration, resulting in a rotational velocity range spanning from 0.9 to 8.9 Hz in 20 s. The corresponding vibration signal Fig. 7(a), measured by the vertical accelerometer, shows an increasing amplitude, as expected in a system dominated by centrifugal forces.

The vibration signal has been processed in parallel by VSDFT and TVDFT, obtaining the diagrams of Fig. 8. Moreover a COT algorithm, based on cubic spline interpolation, has been applied to the same signal, providing a reference for the benchmarking of the two techniques. In Fig. 8(a), a comparison between VSDFT and COT highlights the fidelity of the newly proposed technique, whose transform is almost undistinguishable from the COT result. In particular the dominant components of the signal, superharmonics of the 1st and 2nd order representing two shaft rotational velocities, are not only located correctly on the order axis, but also identified with high precision in terms of amplitude.

On the contrary, Fig. 8(b) shows how the traditional TVDFT introduces a strong distortion in the amplitude of the peaks. It has to be highlighted that the error in the amplitude estimation is not deterministic and varies for the different orders.

The encouraging results of Fig. 8, important for the assessment of the VSDFT/TVDFT effectiveness in very harsh conditions, are however scarcely representative of the real application of such tools in the industrial field. The calculation of the order spectrum for the whole time duration of the acquisition is in fact just an extreme exercise in order to verify the range of application of the VSDFT, and is rarely performed in practice, since it gives just the average amplitude of the signal harmonics in a very wide range of conditions. It is much more common to obtain the so called *waterfall* or *order spectrogram* of the signal, defined as a short time Fourier transform of the signal itself in the angular/order domains. This kind of analysis is also performed online, tracking the vibration amplitudes in real-time and analyzing the data corresponding to the last revolutions of the shaft. In order to demonstrate the effectiveness of the VSDFT, the same test rig of Fig. 6 has been used to track the evolution of vibrations during the acceleration transient displayed in Fig. 9.

Spectrograms have been calculated with the following procedure: (i) time domain signal has been split in sub records corresponding to 10 revolutions of the shaft (thanks to the 1x rev. reference of the tacho signal), with an 8 revolution overlap among sub-records; (ii) each sub-record has been processed independently with cubic-spline COT, TVDFT and VSDFT; (iii) for each sub-record only the orders multiple of 0.1 from 0 to 20 have been saved.

The results are shown in Fig. 10 for the three order-tracking techniques. Since no significant difference is easily identifiable in these diagrams, the amplitude of selected harmonics, obtained by means of TVDFT and VSDFT versus the reference value of COT, is reported as a function of shaft speed in Fig. 11. As displayed in diagrams (a) and (b), respectively related to 0.1 and 0.5 orders, the difference in the results of COT and TVDFT is significant, while VSDFT provides a good estimate of the amplitude of these sub-harmonics, especially at low speed. For orders greater or equal to 1X, as for instance reported in (c) and (d), the two techniques provide very similar results, all matching the COT output.

A second example is provided from a significantly different machine: a Bently Nevada RK4 Rotor Kit. The system is a miniature, bench top rotating machinery able to simulate different aspects of full-scale machinery behavior, such as unbalances and other malfunctions. It consists of a series of three discs, representing most of rotor inertia, installed on a

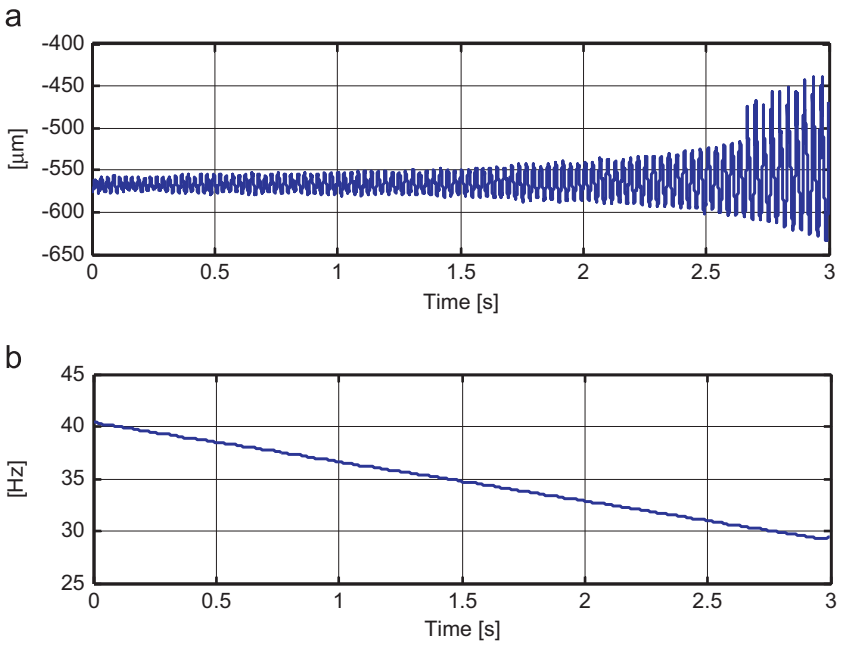

Fig. 12. Experimental test rig 2: (a) proximitor signal, (b) speed profile.

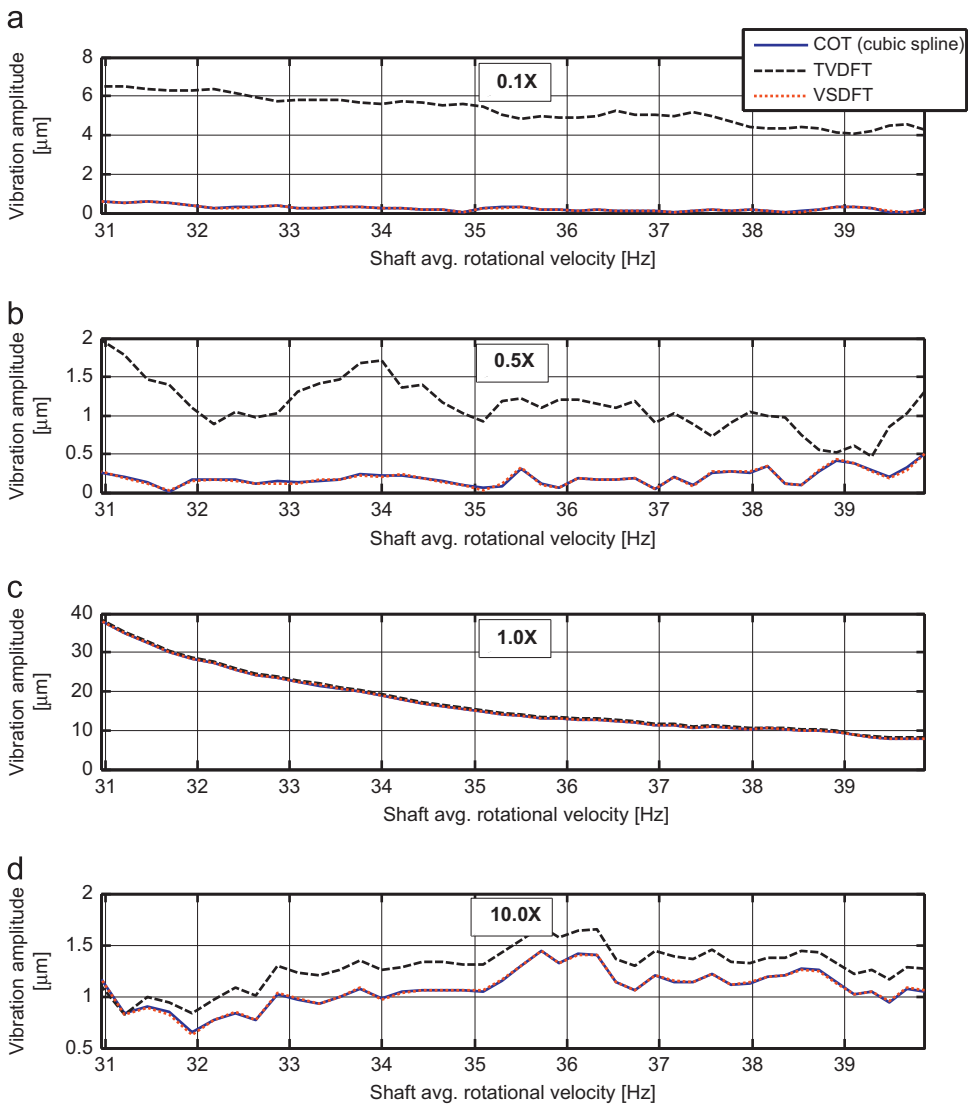

Fig. 13. Experimental test rig 2, amplitude of selected harmonics as a function of shaft speed: (a) 0.1 ×, (b) 0.5 ×, (c) 1 ×, (d) 10 ×.

Fig. 14. Kaplan turbine.

single 10 mm steel shaft. The shaft is mounted on two bushings and is driven by a single phase electric motor. The motor is speed controlled by an auxiliary control system, allowing the manual setting of speed, with a maximum of 10,000 r.p.m., and acceleration, limited to a maximum value of 15,000 rpm/min. The installed sensors include: two proximitors for each bushing, orthogonally installed to measure radial displacements at the bushing housing, and a tachometer, at the driven end of the shaft.

The speed profile of Fig. 12(b) has been obtained by manually decreasing speed on the controller, from an initial value of 40.5 Hz to a final value of 29.4 Hz. This speed profile excited the dynamics of the rotor and Fig. 12(a) shows the resulting vibrations measured by the horizontal proximitor at the non-driven end of the shaft.

Following the same considerations made for the first experimental example, it has been chosen to analyze the evolution of the order spectrum in time. As for the previous example the length of the sliding window has been set to 10 shaft revolutions with an overlap of 8 revolutions.

To assess the effectiveness of the two integral Fig. 13 reports the behavior of the harmonics $0.1\times$ (a), $0.5\times$ (b), $1\times$ (c) and $10\times$ (d), for the three order tracking techniques, as a function of shaft speed. In this case the effectiveness of VSDFT is superior both at low orders and at high orders.

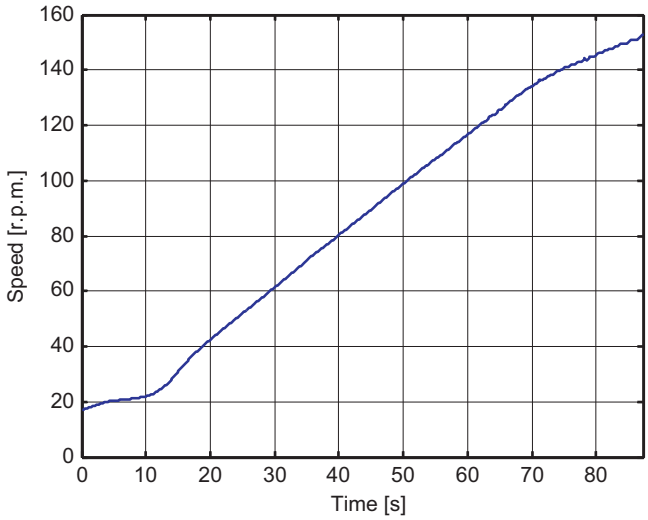

Fig. 15. Kaplan turbine test: shaft velocity during start up.

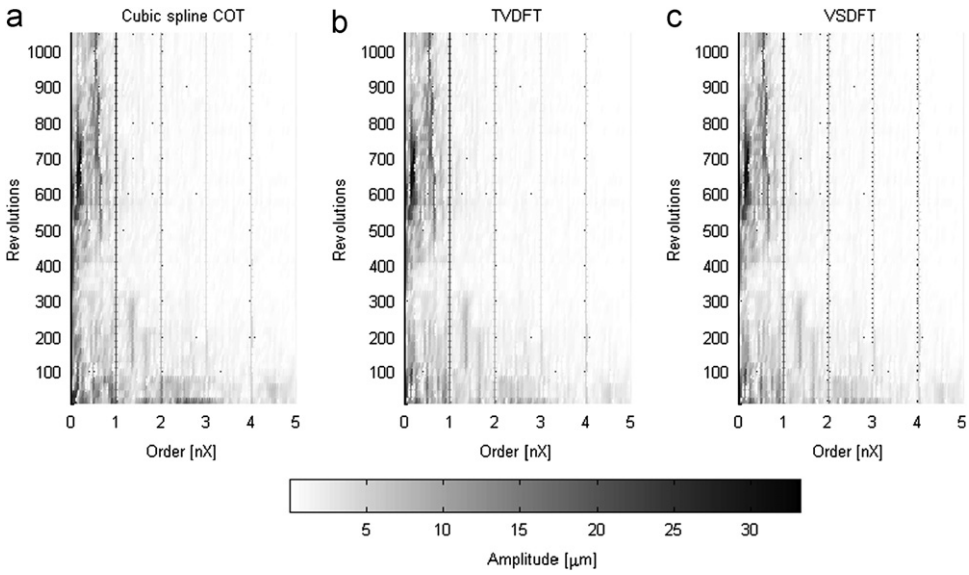

Fig. 16. Kaplan turbine test: order spectrum calculated by means of: (a) cubic spline COT, (b) TVDFT, (c) VSDFT. Sliding observation window length set to 20 revolutions; overlap of 18 revolutions.

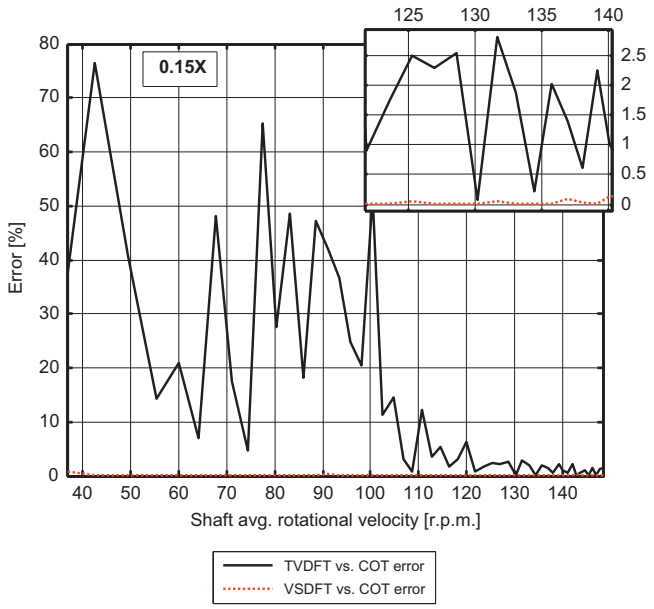

Fig. 17. Kaplan turbine test, relative error in the TVDFT/VSDFT estimates of the 0.15X harmonic vs. the reference value of cubic spline COT.

A third experimental example has been provided in a case where sub-harmonics of the main shaft are important for the diagnostics of hydraulic instabilities. As discussed in [21] the experimental activity has been performed on a Kaplan hydraulic turbine (Fig. 14) coupled to an 18 pole-pairs generator, and equipped with proximitors for vibration measurement. In particular vibrations during the startup have been recorded for the identification of possible hydraulic instabilities. Shaft velocity is reported in Fig. 15. As for the previous experimental examples, the order spectrogram has been calculated, in this case with a sliding window of 20 shaft periods and an 18 period overlap, resulting in the diagrams of Fig. 16, respectively for (a) COT, (b) TVDFT and (c) VSDFT. As noticeable in all those diagrams, a high amplitude phenomenon is happening at low orders ($0.15\times$) between shaft revolution 550 and 750, corresponding approximately to the speed range 120–140 rpm, which can be explained with the insurgence of a hydraulic instability.

A detailed analysis of this significant harmonic component (0.15X), provided in Fig. 17, shows the high fidelity of VSDFT also at low orders: the difference VSDFT-COT remains always below 1%, while the TVDFT estimate is strongly biased, especially at low speeds. Also when the supposed hydraulic instability happens (in the range of speeds 120–140 rpm), the TVDFT vs. COT error fluctuates in the range 2–3%, while the difference VSDFT–COT is always below 0.1% (as shown in the zoom of Fig. 17).

7. Considerations on computational effort

In terms of computational efficiency, a comparison of VSDFT with COT shows that there is no absolute superiority of one technique over the other. In the execution of COT, choosing 2^n number of samples for the interpolated signal, the FFT computation is dominant over the interpolation effort, so the computational effort order will be:

$$Effort_{COT} = O(N\log_2 N) \tag{34}$$

On the other hand the computation of each harmonics in case of VSDFT will be equal to a single frequency DFT (order N), being the VSDFT of Eq. (7) nothing but a DFT with a modified kernel:

$$Effort^1_{VSDFT} = O(N) \tag{35}$$

It is clear that, for the calculations of few harmonics, the VSDFT will have the advantage shown by Eq. (35), whereas the calculation of the whole order spectrum will be by far heavier, since the DFT operation should be repeated for all the N frequencies, leading to a square dependency:

$$Effort^N_{VSDFT} = O(N^2) \tag{36}$$

In the field of diagnostics, especially in the real-time case, few significant harmonic components, related to the velocities of the shafts, are usually considered for the assessment of the health of the machine components. In this case VSDFT can prove more efficient than COT.

Moreover, in real-time applications, the calculations of VSDFT can be updated sample by sample, involving a memory occupation proportional only to the number of harmonics of interest, avoiding the necessity of storing a full set of time samples, as for COT.

8. Conclusions

In this paper a new technique, based on the direct transformation from time to order domain has been proposed. It has been shown analytically and proven numerically and experimentally that, for fast speed variations, it has significant advantages with respect to the traditional TVDFT, with no substantial disadvantage. Indeed, the newly proposed technique can be seen as an improvement of the traditional TVDFT, with the addition of the instantaneous velocity term in the transform expression. The VSDFT shows equivalent quality in the reproduction of the signal in the benchmark with COT. In terms of calculation effort the calculation of the whole order spectrum is less efficient than the one of COT, but VSDFT shows significant advantages in the calculation of amplitudes at single orders. From this point of view, this technique represents a powerful tool, exploiting IAS for the real-time extraction of vibration levels of significant orders for the online diagnostic of rotating machineries.

References

[1] N. Bachschmid, P. Pennacchi, A. Vania, Identification of multiple faults in rotor systems, J. Sound Vibration 254 (2) (2002) 327–366.
[2] R. Ricci, P. Pennacchi, Diagnostics of gear faults based on EMD and automatic selection of intrinsic mode functions, Mech. Syst. Signal Process. 25 (3) (2011) 821–838.
[3] R.B. Randall, J. Antoni, Rolling element bearing diagnostics—a tutorial, Mech. Syst. Signal Process. 25 (2) (2011) 485–520.
[4] J.P. Frazier, J. Page, Phase-lock loop frequency acquisition study, IRE Trans. Space Electron. Telemetr. SET-8 (3) (2011) 210–227.
[5] Weinberg B. Liu, Discrete time analyses of nonuniform sampling first- and second-order digital phase lock loops, IEEE Trans. Commun. 22 (2) (1974) 123–137.
[6] Ferrero R. Ottoboni, High-accuracy Fourier analysis based on synchronous sampling techniques, IEEE Trans. Instrum. Meas. 41 (6) (1992) 780–785.
[7] R.A. Millar, Digital control of shaft speed and position, Spectrum IEEE 5 (1) (1968) 90–95.
[8] R. Potter, M. Gribler, Computed Order Tracking Obsoletes Older Methods, SAE Technical Paper 891131 (1989).
[9] K.R. Fyfe, E.D.S. Munck, Analysis of computed order tracking, Mech. Syst. Signal Process. 11 (2) (1997) 187–205.
[10] J. Stander, P.S. Heyns, Transmission path phase compensation for gear monitoring under fluctuating load conditions, Mech. Syst. Signal Process. 20 (7) (2006) 1511–1522.
[11] H. Vold, M. Mains, J. Blough, Theoretical Foundations for High Performance Order Tracking with the Vold-Kalman Tracking Filter, SAE Technical Paper 972007 (1997).
[12] J. Blough, D. Brown, H. Vold, The time variant discrete Fourier transform as an order tracking method, SAE Paper Number 972006 (1997).
[13] F. Combet, R. Zimroz, A new method for the estimation of the instantaneous speed relative fluctuation in a vibration signal based on the short time scale transform, Mech. Syst. Signal Process. 23 (4) (2009) 1382–1397.
[14] R. Zimroz, J. Urbanek, T. Barszcz, W. Bartelmus, F. Millioz, N. Martin, Measurement of instantaneous shaft speed by advanced vibration signal processing—application to wind turbine gearbox, Metrol. Meas. Syst. 18 (4) (2011) 701–712.
[15] Y. Christos, K. Gryllias, I. Antoniadis, Instantaneous frequency estimation in rotating machinery using a harmonic signal decomposition (HARD) parametric method 2010, in: Proceedings of the ASME IDETC/CIE 2012, August 12–15, 2012.
[16] C. Feldbauer, R. Höldrich, Realization of a Vold–Kalman tracking filter—a least squares problem, in: Proceedings of the COST G-6 Conference on Digital Audio Effects DAFX-00 (2000).
[17] M.C. Pan, C.X. Wu, Adaptive Vold–Kalman filtering order tracking, Mech. Syst. Signal Process. 21 (8) (2007) 2957–2969.
[18] J.R. Blough, A survey of DSP methods for rotating machinery analysis, what is needed, what is available, J. Sound Vibration 262 (2003) 707–720.
[19] G. D'Antona, A. Ferrero, Digital Signal Processing for Measurement Systems, Springer, 2006.
[20] J.A.C. Weideman, Numerical integration of periodic functions: a few examples, The American Mathematical Monthly 109 (1) (2002) 21–36.
[21] P. Pennacchi, P. Borghesani, S. Chatterton, A. Vania, Hydraulic instability onset detection in Kaplan turbines by monitoring shaft vibrations, in: Proceedings of the ASME IDETC/CIE 2012, August 12–15, 2012.